JOURNAL OF SOLID STATE CHEMISTRY 63, 358–368 (1986)

Nature of the Structural Distortion and of the Chemical Bonding in $SnM_3Rh_4Sn_{12}$ (M = La–Gd, Yb, Ca, Sr, and Th)

S. MIRAGLIA, J. L. HODEAU, AND M. MAREZIO

Laboratoire de Cristallographie du CNRS associé à l'Université Scientifique et Médicale de Grenoble, B.P. 166 X, 38042 Genoble Cédex, France

C. LAVIRON[1] AND M. GHEDIRA

Faculté de Sciences et Techniques de Monastir, Monastir, Tunisie

AND G. P. ESPINOSA

AT&T Bell Laboratories, Murray Hill, New Jersey 07974

Received July 18, 1985; in revised form November 25, 1985

The crystal structure of all the $Sn(1)M_3Rh_4Sn(2)_{12}$ compounds (M = La–Gd, Yb, Ca, Sr, and Tb) have been refined from single crystal X-ray diffraction data. Although the compounds with M = La, Ce, Pr, Nd, Sm and Gd have the phase I′ structure the refinements have been carried out by the use of the phase I unit cell. The only significant difference between the two sets of structures lies in the thermal ellipsoid of the Sn(2) atoms. With the exception of the Th compound the major axis of the Sn(2) thermal ellipsoid is on the average 0.06 Å longer for the structures of phase I′ than for those of phase I. The structure of the Th compound exhibits the longest major axis for the Sn(2) thermal ellipsoid, it must contain thus the phase I′ distortion. The absence of the superstructure spots can be explained by a structural disorder. This anomalously long axis has been interpreted as due to a static displacement of the Sn(2) atoms along the Sn(1)–Sn(2) bonds. The distortion from phase I to phase I′ consists thus in a loss of point symmetry of the $Sn(1)Sn(2)_{12}$ polyhedra. A detailed analysis of the variation of the interatomic distances across the series shows that the chemical bonds in these compounds have a covalent/metallic–metallic character as the second-nearest-neighbor interactions are rather strong. However, an electron transfer takes place in these compounds indicating that the bonds have also an appreciable ionic character. The loss of symmetry which takes place when going from phase I to phase I′ is accompanied by a loss of ionic character of the $Sn(1)Sn(2)_{12}$ polyhedra. The Eu^{2+} and Yb^{2+} compounds contain some appreciable amount of Eu^{3+} and Yb^{3+} cations, respectively.

Introduction

Compounds with formulae $SnM_3Rh_4Sn_{12}$ (M = La–Gd, Ca, Sr, Th) and $SnM_4Rh_6Sn_{18}$ (M = Tb–Lu, Y, Sc) have remarkable superconducting and magnetic properties; they become superconducting or undergo a magnetic transition at temperatures lower than ~10 K; the compound with M = Er exhibits reentrant superconductivity (T_c ~ 1 K, Tm ~ 0.5 K) (*1*). Four different phases (I, I′, II, and II′) exist in this system;

[1] Permanent address: division E.F., CERN, 1211 Genève 23, Switzerland.

0022-4596/86 $3.00

phases I and I′ correspond to the chemical formula $Sn(1)M_3Rh_4Sn_{12}$ (*2–4*). Phase I is cubic (space group $Pm3n$, $a_I \simeq 9.7$ Å) and exists for M = Eu, Yb, Ca, Sr, and Th. Phase I′ is a distortion of phase I and exists for M = La–Gd; the symmetry is either body-centered cubic with $a_{I'} \sim 2a_I$ or tetragonal with $a_{I'} \sim a_I\sqrt{2}$ and $c_{I'} \sim a_I$. Since the distortion of phase I′ with respect to phase I is very small, the two phases have similar structural arrangements. Phases II and II′ correspond to the chemical formula $Sn(1)M_4Rh_6Sn_{18}$; in these phases some or all Sn(1) atoms may be replaced by M atoms. Phase II is tetragonal with $a_{II} \sim 13.75$ Å and $c_{II} \sim 27.4$ Å and exists for M = Ho–Lu, Y, and Sc; phase II′ is a disordered microtwinned phase II and exists for M = Tb–Tm (*5, 6*).

The structures of all these phases contain a three-dimensional network of corner-sharing $RhSn_6$ trigonal prisms. In the structure of phases I and I′, this network generates icosahedral and cubooctahedral sites which are occupied by the Sn(1) and M atoms. These two atoms form a sublattice having the arrangement of an A15 structure. Since the 12-coordinated icosahedral and cubooctahedral sites have approximately the same size, a disorder between the Sn(1) and M atoms could take place. As stated above the distortion of the phase I′ structure with respect to that of the phase I, is very small. Exposure times greater than 200 hr were necessary to observe the superstructure reflections by the use of a single crystal, a precession camera, and Mo$K\alpha$ radiation (*4*). It is, thus, a good approximation to describe the structure of phase I′ compounds by using the phase I unit cell ($a_I \sim 9.7$ Å) and its space group ($Pm3n$). This article reports the results of the structural refinements for all the compounds having either the phase I or the phase I′ structure. These refinements have been carried out by assuming that the compounds have the phase I structure. A comparison between these structures has allowed us to infer the main features of the phase I′ distortion and to have a qualitative view about the nature of the chemical bonds.

Experimental

All single crystals of the compounds described herein were grown by dissolving the constituents in an excess of tin with a controlled temperature held at ~1050°C for ~2 hr; a cooling rate of 5–10°C/hr was initiated down to ~550°C. Details about the crystal growth process are reported in Ref. (*7*).

The symmetry of the crystals as well as their quality were checked by a precession camera and Mo$K\alpha$ radiation. It was confirmed that the compounds with M = Eu, Yb, Ca, Sr, and Th crystallize with the phase I structure, namely all reflections could be indexed on a cubic cell of ~9.7 Å, and the systematic absences (hhl for $l = 2n + 1$) corresponded to the $Pm3n$ space group. Instead, the precession photographs for the compounds with M = La, Ce, Pr, Nd, Sm and Gd showed that the corresponding crystals had the phase I′ structure. They contained weak superstructure spots which could be indexed on either a body-centered cubic cell with $a_I \sim 2a_I$ or a tetragonal cell with $a_{I'} \sim a_I\sqrt{2}$ and $c_{I'} \sim a_I$. The systematic absences lead to the space groups given in Ref. (*4*). In the case of the tetragonal indexing the sample would consist of a triple-twinned crystal in which the twinning elements would correspond to the four threefold [111] axes of the pseudocubic cell. Form the intensity distribution of the superstructure reflections in the X-ray photographs it can be concluded that the phase I′ distortion is mainly a displacing distortion.

The intensity data collections were carried out by the use of spherical samples and a four-circle diffractometer equipped either with Ag$K\alpha$ or Mo$K\alpha$ radiation and graphite monochromator. The sample radii are given in Table I. They represent the average val-

TABLE I

INTENSITY COLLECTION AND REFINEMENT PARAMETERS

M	La	Ce	Pr	Nd	Sm	Gd	Th	Eu	Yb	Ca	Sr
Radiation	Mo*Kα*	Ag*Kα*	Ag*Kα*	Ag*Kα*	Ag*Kα*	Mo*Kα*	Mo*Kα*	Mo*Kα*	Ag*Kα*	Ag*Kα*	Ag*Kα*
Scan type	ω	ω	ω/Θ	ω	ω	ω	ω	ω	ω	ω	ω
Speed variable (deg/sec)	0.01 0.04	0.02 0.08	0.005 0.01	0.02 0.06	0.02 0.06	0.01 0.04	0.01 0.04	0.01 0.04	0.02 0.08	0.02 0.06	0.02 0.06
Scan width A	1.5	1.6	1.0	1.4	1.4	1.5	1.5	1.5	1.5	1.4	1.4
Scan width B	0.2	0.2	0.45	0.2	0.2	0.2	0.2	0.2	0.2	0.2	0.2
Detector aperture A	1.0	2.0	2.0	1.0	1.0	1.0	1.0	1.0	1.0	1.0	1.0
Detector aperture B	1.5	1.5	2.0	1.5	1.5	1.5	1.5	1.5	1.5	1.5	1.5
θ range	5–35	3–32	5–25	13–32	13–32	5–35	5–35	5–35	3–30	3–31	13–32
No. of collected reflections	3886	2207	6217	2482	2268	3525	5060	3679	15932	9086	3244
No. of independent reflections (*m*3*m*)	459	577	369	539	500	443	458	454	375	620	529
No. of reflections used in the refinement	268	120	177	354	283	229	214	248	269	306	366
μR	4.8	1.65	1.32	1.45	1.48	3.9	3.6	3.8	2.4	1.06	1.44
Radius (cm)	0.0176	0.0114	0.0090	0.0096	0.0093	0.0120	0.0080	0.0124	0.013	0.0096	0.0095
R	0.028	0.026	0.036	0.030	0.024	0.024	0.025	0.018	0.016	0.017	0.022
wR	0.029	0.028	0.028	0.034	0.027	0.023	0.024	0.019	0.015	0.016	0.024
a (Å)	9.745(1)	9.708(1)	9.698(2)	9.675(3)	9.656(2)	9.638(1)	9.692(1)	9.749(1)	9.676(1)	9.705(2)	9.801(2)

ues as the sample sphericity varied within 10%. The integrated intensities were measured by the ω-scan technique with a variable scan width given by $\delta\theta = A + B \tan\theta$ and a variable speed according to the intensity. For all compounds only the reflections corresponding to the phase I cell were measured. The detailed experimental conditions for each compound are reported in Table I. The integrated intensities were first averaged in the *m*3*m* point group and then converted into structure factors by applying the Lorentz, polarization, and absorption corrections. A comparison between observed and calculated structure factors revealed that strong reflections occurring at low angle θ values were highly affected by extinction. Since the number of parameters to be refined was rather small (one scale factor, two positional parameters, nine temperature factors, and eventually two occupancy factors), the number of independent reflections was quite large, and the form factors of all atoms were about the same order of magnitude, the extinction effects were minimized by excluding from the refinements all reflections occurring at low θ angles. The limits of 0.54 and 0.40 for $\sin\theta/\lambda$ were taken for the compounds with *M* = Ca, Yb, Pr and *M* = La, Ce, Nd, Sm, Gd, Th, Sr, Eu, respectively. Moreover, the weak reflections corresponding to $F^2 < 10\sigma(F^2)$ were also excluded from the refinements. The weighting scheme $1/\sigma(F)^2$ was used throughout the refinements. As the coordination number and the size of the Sn(1) and *M* sites are the same, a disorder between these two atoms is possible. In the last stage of the refinement the disorder was simulated by varying the occupancy factor of the two sites. The departures of the two occupancy factors from unity were in all cases smaller than three times the standard deviations, which indicated that if a substitution takes place between these two sites, it is rather small. An upper limit for the disorder of about 3% can be estimated as variations of the occupancy factors within this limit do not correspond to any variations of the *R* and *wR* factors. The final positional and thermal parameters for all compounds are reported in Table II while the *R* and *wR* factors are reported in Table I.

The lattice parameters were determined by X-ray powder data and their values were

TABLE II

POSITIONAL AND THERMAL PARAMETERS

Compound	Atoms	Positions	Point symmetry	x	y	z	β_{11}	β_{22}	β_{33}	β_{12}	β_{13}	β_{23}
$Sn(1)La_3Rh_4Sn_{12}$	Sn(1)	2a	$m3$	0	0	0	.00304(7)	—	—	0	0	0
	La	6d	$42m$	¼	½	0	.00207(6)	.00151(3)	—	0	0	0
	Rh	8e	32	¼	¼	¼	.00125(3)	—	—	−.00001(7)	—	—
	Sn(2)	24k	m	0	.30555(10)	.15376(6)	.00116(3)	.00915(7)	.00230(4)	0	0	.00506(9)
$Sn(1)Ce_3Rh_4Sn_{12}$	Sn(1)	2a	$m3$	0	0	0	.0028(4)	—	—	0	0	0
	Ce	6d	$42m$	¼	½	0	.00186(9)	.0015(1)	—	0	0	0
	Rh	8e	32	¼	¼	¼	.0012(1)	—	—	.0001(4)	—	—
	Sn(2)	24k	m	0	.3070(2)	.1537(1)	.00102(5)	.0088(1)	.00225(6)	0	0	.0052(1)
$Sn(1)Pr_3Rh_4Sn_{12}$	Sn(1)	2a	$m3$	0	0	0	.00299(9)	—	—	0	0	0
	Pr	6d	$42m$	¼	½	0	.00217(7)	.00151(4)	—	0	0	0
	Rh	8e	32	¼	¼	¼	.00120(4)	—	—	−.00002(7)	—	—
	Sn(2)	24k	m	0	.30730(11)	.15354(7)	.00107(4)	.00849(8)	.00219(5)	0	0	.00233(11)
$Sn(1)Nd_3Rh_4Sn_{12}$	Sn(1)	2a	$m3$	0	0	0	.0031(2)	—	—	0	0	0
	Nd	6d	$42m$	¼	½	0	.00234(5)	.00159(5)	—	0	0	0
	Rh	8e	32	¼	¼	¼	.00124(7)	—	—	−.0001(2)	—	—
	Sn(2)	24k	m	0	.30763(9)	.15360(6)	.00117(3)	.00828(6)	.00229(3)	0	0	.00453(8)
$Sn(1)Sm_3Rh_4Sn_{12}$	Sn(1)	2a	$m3$	0	0	0	.0033(2)	—	—	0	0	0
	Sm	6d	$42m$	¼	½	0	.00259(5)	.00181(5)	—	0	0	0
	Rh	8e	32	¼	¼	¼	.00136(7)	—	—	−.0002(2)	—	—
	Sn(2)	24k	m	0	.30829(9)	.15345(6)	.00135(3)	.00814(6)	.00240(3)	0	0	.00434(9)
$Sn(1)Gd_3Rh_4Sn_{12}$	Sn(1)	2a	$m3$	0	0	0	.00342(8)	—	—	0	0	0
	Gd	6d	$42m$	¼	½	0	.00278(6)	.00199(3)	—	0	0	0
	Rh	8e	32	¼	¼	¼	.00144(3)	—	—	.00000(8)	—	—
	Sn(2)	24k	m	0	.30854(10)	.15332(3)	.00134(3)	.00843(6)	.00251(4)	0	0	.00461(10)
$Sn(1)Th_3Rh_4Sn_{12}$	Sn(1)	2a	$m3$	0	0	0	.00325(10)	—	—	0	0	0
	Th	6d	$42m$	¼	½	0	.00243(5)	.00186(3)	—	0	0	0
	Rh	8e	32	¼	¼	¼	.00171(4)	—	—	−.00003(11)	—	—
	Sn(2)	24k	m	0	.30774(13)	.15270(10)	.00146(5)	.01046(10)	.00376(6)	0	0	.00805(14)
$Sn(1)Yb_3Rh_4Sn_{12}$	Sn(1)	2a	$m3$	0	0	0	.0040(1)	—	—	0	0	0
	Yb	6d	$42m$	¼	½	0	.00264(2)	.00213(3)	—	0	0	0
	Rh	8e	32	¼	¼	¼	.00151(4)	—	—	−.0001(1)	—	—
	Sn(2)	24k	m	0	.30570(4)	.15333(3)	.00144(2)	.00503(2)	.00211(2)	0	0	.00263(4)
$Sn(1)Eu_3Rh_4Sn_{12}$	Sn(1)	2a	$m3$	0	0	0	.00341(6)	—	—	0	0	0
	Eu	6d	$42m$	¼	½	0	.00219(4)	.00176(2)	—	0	0	0
	Rh	8e	32	¼	¼	¼	.00136(20	—	—	−.00008(6)	—	—
	Sn(2)	24k	m	0	.30256(6)	.15358(5)	.00133(3)	.00467(4)	.00193(3)	0	0	.00146(6)
$Sn(1)Ca_3Rh_4Sn_{12}$	Sn(1)	2a	$m3$	0	0	0	.00359(9)	—	—	0	0	0
	Ca	6d	$42m$	¼	½	0	.00274(9)	.00228(11)	—	0	0	0
	Rh	8e	32	¼	¼	¼	.00140(3)	—	—	−.00017(9)	—	—
	Sn(2)	24k	m	0	.30361(3)	.15338(3)	.00137(1)	.00462(2)	.00196(1)	0	0	.00125(3)
$Sn(1)Sr_3Rh_4Sn_{12}$	Sn(1)	2a	$m3$	0	0	0	.00313(13)	—	—	0	0	0
	Sr	6d	$42m$	¼	½	0	.00243(6)	.00181(6)	—	0	0	0
	Rh	8e	32	¼	¼	¼	.00131(5)	—	—	−.0001(1)	—	—
	Sn(2)	24k	m	0	.29986(5)	.15342(2)	.00127(2)	.00487(3)	.00191(2)	0	0	.00159(5)

reported in Table I. Furthermore for each crystal mounted on the four-circle diffractometer, the θ values of 25 high-angle reflections were measured; the lattice parameters determined by least-squares are in good agreement with the values reported in Table I and with those reported in Ref. (*1*) determined from X-ray powder data. Values reported in Table I were used together with the positional parameters to calculate the interatomic distances and angles reported in Table III. The thermal data are given in Table IV.

Discussion

There are no appreciable shifts in the positional parameters between the compounds having the phase I structure and those having the phase I′ structure. They all agree very well with the positional parameters of $Sn(1)Yb_3Rh_4Sn_{12}$ reported in Ref. (*3*). Consequently the interatomic distances and angles vary less than 2% and 2° (in most cases less than 1°), respectively, on going from one compound to the next. On the other hand, small but significant differences exist in the thermal data of these compounds. Their analysis allows the determination of the important features for the phase I′ distortion.

It can be seen from Table IV that a significant difference exists for the major axis of the Sn(2) thermal ellipsoid between the compounds with M = Eu, Yb, Ca, and Sr (phase I) and those with M = La, Ce, Pr, Nd, Sm, and Gd (phase I′). It is on the average 0.15 Å for the former compounds and 0.21 Å for the latter. The compound with M = Th is unique, as it crystallizes with the structure of phase I, but the major axis of the Sn(2) thermal ellipsoid is the largest (0.242 Å) among the eleven compounds reported in this article. The other thermal data are practically the same for all compounds. Since the structure of the phase I′ compounds has been refined in a more symmetrical space group (the superstructure spots have not been taken into account), the 40% increase of one of the thermal-ellipsoid axes correspond to a static distortion rather than to an actual increase of the thermal motion.

In the phase I′ compounds the major axis of the Sn(2) thermal ellipsoid makes an angle of about 18° with the b axis and one of about 12° with the direction of the Sn(1)–Sn(2) bond. In the phase I compounds the corresponding angles are 14° and 16°, respectively. Figures 1a and b show the projections on the xy plane of phase I′ and I structures while Fig. 1c shows that of the Th-compound structure. The atoms are

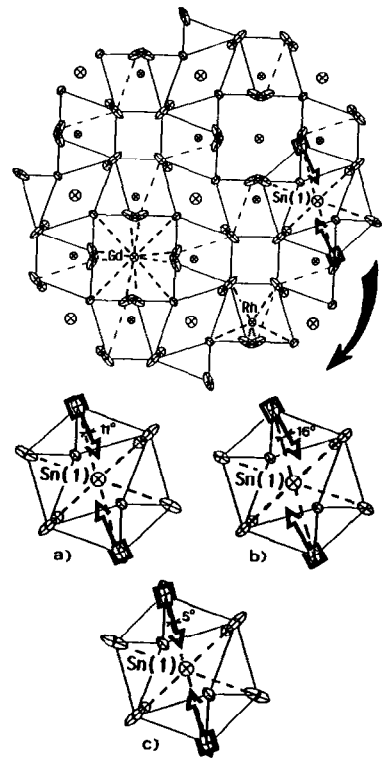

FIG. 1. Three-dimensional arrangement of the $Sn(1)M_3Rh_4Sn(2)_{12}$ structures: the Sn(1) polyhedron is shown (a) for phase I′ (M = Gd), (b) for phase I (M = Eu), and (c) for the Th compound. Atoms are represented by their thermal ellipsoids.

TABLE III

INTERATOMIC DISTANCES[a] (Å) AND ANGLES (°)

	La	Ce	Pr	Nd	Sm	Gd	Th	Eu	Yb	Ca	Sr
Sn(1) Icosahedron											
Sn(1)–Sn(2) × 12	3.333	3.334	3.331	3.327	3.326	3.321	3.330	3.308	3.309	3.301	3.301
Sn(2)–Sn(2) × 6	2.997/53.42	2.984/53.17	2.978/53.10	2.972/53.06	2.964/52.93	2.955/52.85	2.960/52.78	2.995/53.82	2.967/53.27	2.977/53.61	3.007/54.19
Sn(2)–Sn(2) × 24	3.647/66.33	3.651/66.41	3.650/66.43	3.646/66.44	3.646/66.49	3.642/66.51	3.653/66.54	3.613/66.20	3.623/66.38	3.609/66.27	3.599/66.08
M Cubooctahedron											
M–Sn(2) × 4	3.417	3.408	3.406	3.398	3.394	3.389	3.412	3.416	3.397	3.404	3.431
M–Sn(2) × 8	3.431	3.410	3.404	3.395	3.384	3.376	3.396	3.448	3.404	3.426	3.480
Sn(2)–Sn(2) × 4	2.997/51.79	2.984/51.89	2.978/51.88	2.972/51.92	2.864/51.94	2.955/51.92	2.960/51.67	2.995/51.48	2.967/51.68	2.977/51.51	3.007/51.19
Sn(2)–Sn(2) × 8	3.647/64.35	3.651/64.76	3.650/64.82	3.646/64.92	3.646/65.09	3.642/65.15	3.653/64.89	3.613/63.52	3.623/64.37	3.609/63.79	3.599/62.77
Sn(2)–Sn(2) × 4	3.790/67.05	3.747/66.66	3.738/66.60	3.723/66.50	3.703/66.33	3.691/66.28	3.727/66.55	3.850/67.87	3.760/67.05	3.812/67.61	3.923/68.61
Sn(2)–Sn(2) × 8	3.271/57.06	3.244/56.81	3.238/56.78	3.226/56.72	3.214/56.62	3.207/56.60	3.241/56.84	3.308/57.63	3.251/57.11	3.284/57.47	3.358/58.13
Trigonal prism											
Rh–Sn(2) × 6	2.666	2.660	2.657	2.652	2.648	2.644	2.660	2.662	2.649	2.653	2.671
Sn(2)–Sn(2) × 6	3.647/86.30	3.651/86.69	3.650/86.75	3.646/86.84	3.646/87.00	3.642/87.05	3.653/86.75	3.613/85.46	3.623/86.28	3.609/85.72	3.599/84.70
Sn(2)–Sn(2) × 3	3.271/75.68	3.244/75.14	3.238/75.07	3.226/74.93	3.214/74.72	3.207/74.65	3.241/75.07	3.308/76.83	3.251/75.71	3.284/76.48	3.358/77.88
Other distances											
Rh–*M*	3.445	3.433	3.429	3.421	3.414	3.407	3.427	3.447	3.421	3.431	3.465
Sn(1)–Rh	4.220	4.205	4.199	4.190	4.182	4.173	4.197	4.221	4.190	4.202	4.244
Sn(1)–*M*	5.448	5.428	5.421	5.409	5.398	5.388	5.418	5.450	5.409	5.425	5.478

[a] In all cases the standard deviation is less than 0.001 Å.

TABLE IV

THERMAL DATA: ROOT-MEAN-SQUARE VALUES (Å)

		La	Ce	Pr	Nd	Sm	Gd	Th	Eu	Yb	Ca	Sr
Sn(1)	r	.121	.116	.119	.123	.125	.127	.124	.128	.137	.131	.123
M	r_1	.100	.094	.102	.105	.111	.114	.108	.103	.112	.114	.109
	r_2	.085	.085	.085	.087	.093	.097	.094	.092	.100	.104	.094
	r_3	.085	.085	.085	.087	.093	.097	.094	.092	.100	.104	.094
Rh	r_1	.077	.077	.076	.078	.082	.082	.091	.082	.086	.084	.082
	r_2	.077	.073	.076	.078	.082	.082	.091	.082	.086	.084	.082
	r_3	.077	.073	.074	.078	.075	.082	.089	.078	.082	.076	.076
Sn(2)	r_1	.219	.215	.210	.207	.205	.208	.242	.153	.158	.151	.157
	r_2	.084	.080	.082	.085	.089	.090	.094	.092	.095	.093	.091
	r_3	.075	.070	.071	.074	.080	.079	.083	.080	.082	.081	.079
Sn(2)	x	90	90	90	90	90	90	90	90	90	90	90
major axis	y	18.2	19.3	18.3	18.6	18.6	18.9	25.1	14.0	14.6	12.6	14.1
angle with	x	71.8	70.7	71.7	71.4	71.4	71.1	64.9	76.0	75.4	77.4	75.9
M valence		3^+	3^+	3^+	3^+	3^+	3^+	4^+	2^+	2^+	2^+	2^+

represented by their thermal ellipsoids. It can be seen that in general the major axis of the Sn(2) atoms is perpendicular to the Rh–Sn(2) and M–Sn(2) bonds. Therefore, the distortion of the phase I′ structures consists mainly in the displacement of the Sn(2) atoms along the Sn(1)–Sn(2) bonds. The Sn(2) icosahedra around the Sn(1) atoms lose the $m3$ point symmetry and the 12 Sn(1)–Sn(2) distances are not equal anymore.

By comparing the results of the Th compound with those of the other compounds it can be surmised that the structure of $SnTh_3Rh_4Sn_{12}$ has the phase I′ distortion. The major axis of the Sn(2) thermal ellipsoid of the Th compound is ~25% larger than the corresponding value of the La, Ce, Pr, Nd, Sm, and Gd compounds and it forms an angle of ~5° with the direction of the Sn(1)–Sn(2) bond. The absence of the superstructure spots can be explained if in the Th compound the distortion is not long range. Furthermore, since electron diffraction photographs failed to reveal the presence of any diffuse scattering streaks, it can be concluded that the distortion is completely disordered.

In Fig. 2 the lattice parameters of $SnM_3Rh_4Sn_{12}$ compounds with M = La–Gd, Yb are plotted as function of atomic number. It is clear that the Eu and Yb atoms are in a different valence state than the other rare earth atoms. This observation and the way the coordination polyhedra are arranged in the structure lead to the conclusion that these compounds have a strong covalent/ionic character rather than a pure metallic one. The Sn(1), M, and Rh atoms have

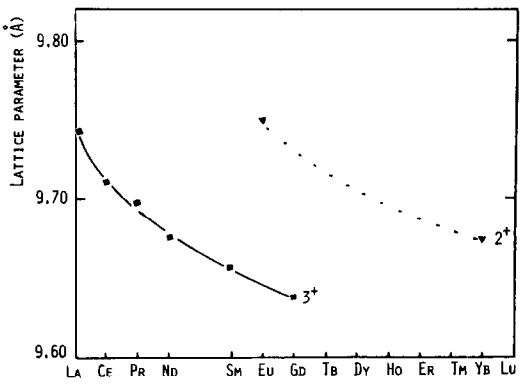

FIG. 2. Lattice parameters of the $Sn(1)M_3Rh_4Sn(2)_{12}$ compounds (M = rare-earth cations) as functions of atomic number. The superstructure for the M^{3+} compounds has not been taken into account.

a cation behavior while the Sn(2) atoms have an anion behavior. It is reasonable to assume that the Eu, Yb, Ca, and Sr atoms are in the divalent state, the La, Ce, Pr, Nd, Sm, and Gd atoms are in the trivalent state, and the Th atoms are in the tetravalent state. The structural analysis of the entire series corroborates the idea that an electron transfer takes place between the different sites. Figure 3 shows the variation of the Rh–Sn(2), Sn(1)–Sn(2), and *M*–Sn(2) distances across the series. The variation of the shortest Sn(2)–Sn(2) distance is also shown. The values of these distances are plotted against the lattice parameters of the various compounds. For the Rh–Sn(2) distances there exists a curve for each valence of the *M* atom, which means that the Rh-site size depends upon the valence of the *M* atoms. This strongly indicates that the Rh atoms carry a cation charge. The most stable valence states for the Rh atoms are the trivalent and the tetravalent states. As the *M* valence increases the number of Rh^{4+} decreases while that of Rh^{3+} increases and consequently the value of the Rh–Sn(2) distance increases. It can be seen from Fig. 3 that the variation of the Rh–Sn(2) and Sn(1)–Sn(2) distances across the series is not the same. The Rh–Sn(2) distance increases and the Rh valence decreases on going from M^{2+} to M^{3+} and to M^{4+}. The Sn(1)–Sn(2) distance increases and the Sn(1) valence decreases only when the *M* valence increases from 2+ to 3+, while they remain constant on going from M^{3+} to M^{4+}. In fact the Sn(1)–Sn(2) distance of the Th^{4+} compound falls on the curve of the M^{3+} compounds. This means that in the Th^{4+} compound, the additional electron transfer takes place only toward the Rh sites. In truly ionic compounds the average cation–anion distance does not vary appreciably if a third constituent of the structure is substituted. For example, in the rare-earth orthoferrites, $REFeO_3$, the average Fe–O distance across the series remains practically unchanged (*8*). In the stannides, the cation–anion distances Sn(1)–Sn(2) for M^{3+} and Rh–Sn(2) for M^{3+} and M^{2+} increase with increasing rare-earth atom radius, which indicates that the interactions between second-nearest neighbor have an appreciable effect on the interatomic distances. Such behavior is typical of covalent/metallic compounds. On the contrary, in ionic compounds second-nearest-neighbor interactions (cation–cation) have a negligible effect on first-nearest-neighbor distances (cation–anion) because of the screening effect due to the anion network. It is worth pointing out that the Sn(1)–Sn(2) distances for the M^{2+} compounds exhibit a unique variation across the series. The same value (3.301 Å) has been found for the compounds of the two alkaline-earth cations (Ca^{2+} and Sr^{2+}) while 3.308 and 3.309 Å have been found for those of the two rare-earth cations Eu^{2+} and Yb^{2+}, respectively. Such a behavior can be interpreted as an indication that the Sn(1)–$Sn(2)_{12}$ polyhedra in these compounds have an ionic character and that the Eu and Yb compounds contain a certain amount of Eu^{3+} and Yb^{3+} cations. The distortion from phase I to phase I′ is accompanied by a decrease of the ionic character of the $Sn(1)Sn(2)_{12}$ polyhedra. The two points corresponding to the alkaline-earth cations are on one side of the curve whereas those corresponding to the two rare-earth cations are on the other for most of the other distances. The separation is clear-cut only for the Sn(1)–Sn(2) distances while for all the others it is about within one or two standard deviations. With only four points it is rather difficult to see this difference; however, it should be noticed that the values corresponding to the divalent rare-earth cations are always in between those corresponding to the trivalent rare-earth cations and those corresponding to the divalent alkaline-earth cations. This strongly corroborates the assumption that the Eu and Yb

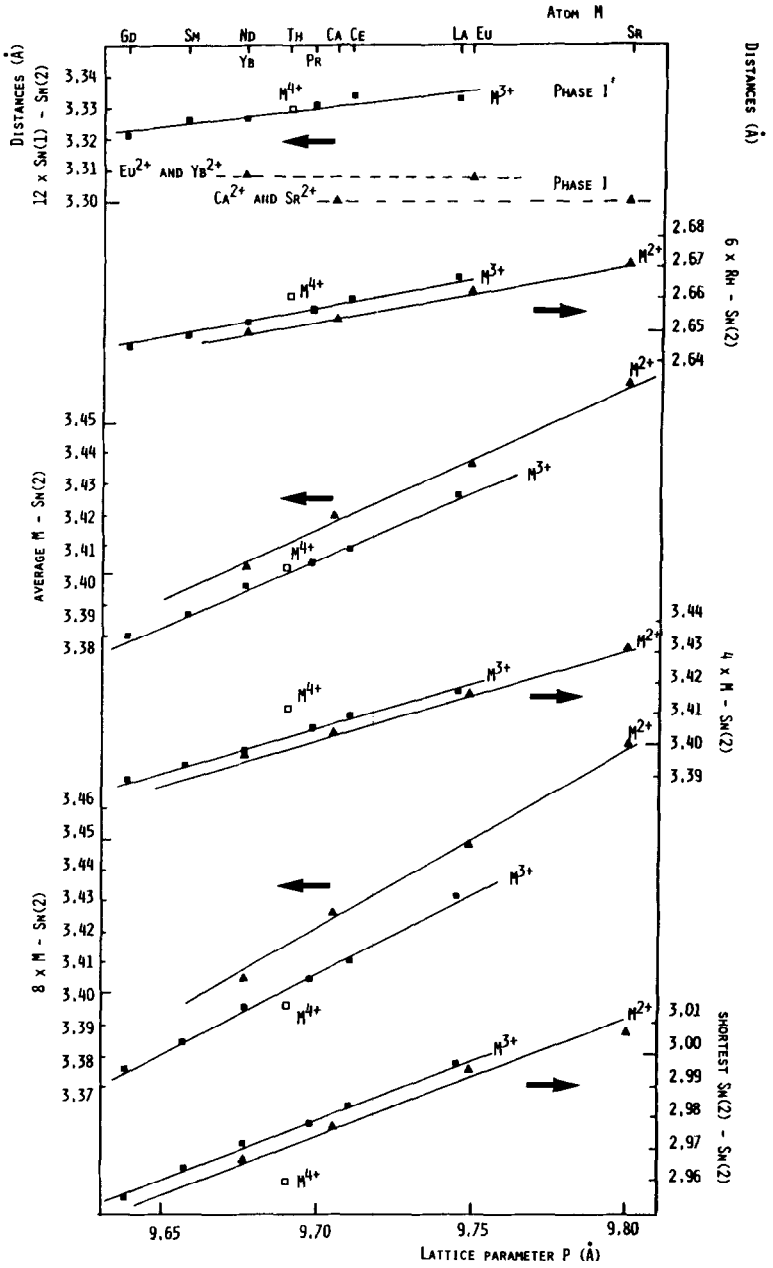

FIG. 3. Variation across the series of the Sn(1)–Sn(2), the Rh–Sn(2), the *M*–Sn(2), and the shortest Sn(2)–Sn(2) distances. The primitive cubic lattice parameters are reported along the abscissae.

compounds contain some Eu^{3+} and Yb^{3+} cations, respectively.

The *M* atoms occupy cubooctahedral sites having a $\bar{4}2m$ point symmetry. The 12 *M*–Sn(2) distances comprise two groups of four and eight equal distances, respectively. For both groups of distances there exists a curve for each valence of the *M*

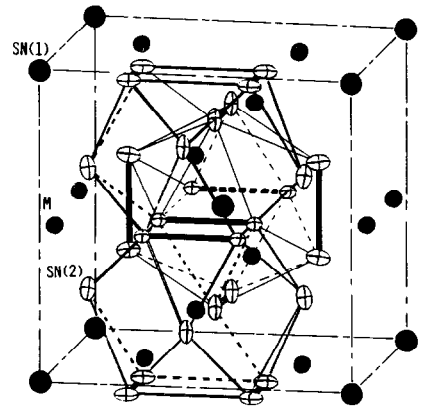

FIG. 4. The A15 sublattice of Sn(1)M_3. The coordination polyhedra around one Sn(1) and two M atoms are represented. The shortest Sn(2)–Sn(2) distances are indicated by heavy lines.

atoms. The value of the eight M–Sn(2) distances decreases with increasing valence of the M atoms which is a normal behavior as cation size decreases with increasing valence. On the contrary, the value of the four M–Sn(2) distances increases with increasing valence of the M atoms. This anomalous behavior is due to second-nearest-neighbor interactions. As can be seen from Fig. 3 the average of the 12 distances decreases with increasing valence of the M atoms, however, the value of the Th compound falls on the curve of the M^{3+} compounds.

The variation of the shortest Sn(2)–Sn(2) distance is shown in Fig. 3. This distance varies between 2.955 and 3.007 Å while all the other Sn(2)–Sn(2) distances are greater than ~3.20 Å. It forms two edges of each rectangle shared by the infinite M-cubooctahedron chains and it is also a shared edge between the M cubooctahedra and the Sn(1) icosahedra (Fig. 4). The variation of this distance across the series gives rise to three curves, one for each M valence, however, the sequence of the three curves is not as expected. The shortest Sn(2)–Sn(2) distance decreases on going from the M^{3+} to the M^{2+} and to the M^{4+} compounds. The Sn(2) atoms are coordinated to one Sn(1), three M, and two Rh atoms. The valence variations of the M and Sn(1) atoms have opposite effects on the Sn(2)–Sn(2) short distances. When the M valence increases from 2+ to 3+ the M-site size decreases and the Sn(2)–Sn(2) edges tend to decrease. At the same time, because of the electron transfer, the Sn(1) valence decreases, the Sn(1)-site size increases, and the Sn(2)–Sn(2) edges tend to increase. This indicates that on going from M^{2+} to M^{3+} the increase of the Sn(1)-site size prevails over the decrease of the M-site size. As stated above the valence of the Sn(1) site does not change when going from M^{3+} to M^{4+}. In this case only the decrease of the M-site size has an effect on the Sn(2)–Sn(2) distances and a decrease of the shortest Sn(2)–Sn(2) distance is observed. We have not taken into account the variation of the Rh-site size. Since the shortest Sn(2)–Sn(2) distance is not an edge of the trigonal prisms surrounding the Rh atoms, the size variation of the Rh sites has a negligible effect on this distance.

The valence of the M sites is a very important factor for the crystal chemistry of the $SnM_3Rh_4Sn_{12}$ series. As stated above the structure of the M^{3+} compounds is distorted with respect to that of the M^{2+} compounds and the structure of the Th^{4+} compound is also distorted, but the distortion is not ordered. The main feature of the distortion is a loss of point symmetry for the Sn(1) sites. When the M^{2+} atoms are replaced by M^{3+} or M^{4+} atoms, the Sn(1) valence decreases. Consequently the Sn(1)–Sn(2) bond strength decreases, the Sn(1) polyhedron undergoes a distortion, and the crystal symmetry decreases.

The increase of the Sn(1)–Sn(2) distances when going from M^{2+} to M^{3+} is ~0.025 Å while the corresponding increase of the Rh–Sn(2) distances is only 0.005 Å. The in-

crease of the former distances is larger because in the I′ structures, that is, the compounds with M^{3+} and M^{4+}, the distortion of the Sn(1) sites brings about an additional site-size increase. It is well known that distorted coordination polyhedra correspond to larger average interatomic distances.

The analogy from the structural point of view between the $SnM_3Rh_4Sn_{12}$ and the $A'A''_3B_4O_{12}$ compounds has been discussed in Ref. (*3*). The latter compounds have a perovskite-like structure in which an order 1 : 3 exists on the 12-coordinated sites. By a simple mechanism similar to that by which a NiAs structure transforms into a NaCl one, the Rh_4Sn_{12} network can be transformed into the B_4O_{12} network. The stannides can then be considered as the covalent counterparts of the $A'A''_3B_4O_{12}$ perovskites. The isostructural relationship between $Na[Mn_3^{3+}](Mn_2^{3+}Mn_2^{4+})O_{12}$ and $Ca[Cu_3^{2+}](Mn_4^{4+})O_{12}$ (*9*, *10*) is similar to that existing between $SnLa_3^{3+}Rh_4Sn_{12}$ and $Sn\,Eu_3^{2+}Rh_4Sn_{12}$. This isormorphism by electron transfer which can exist in both series is another point of analogy between the two series.

References

1. J. P. Remeika, G. P. Espinosa, A. S. Cooper, H. Barz, J. M. Rowell, D.B. McWhan, J. M. Vandenberg, D. E. Moncton, Z. Fisk, L. D. Woolf, H. C. Hamaker, M. B. Maple, G. Shirane, and W. Thomlinson, *Solid State Commun.* **34,** 923 (1980).
2. J. M. Vandenberg, *Mater. Res. Bull.* **15,** 835 (1980).
3. J. L. Hodeau, J. Chenavas, M. Marezio, and J. P. Remeika, *Solid State Commun.* **36,** 839 (1980).
4. J. L. Hodeau, M. Marezio, J. P. Remeika, and C. H. Chen, *Solid State Commun.* **42,** 97 (1982).
5. J. L. Hodeau, M. Marezio, and J. P. Remeika, *Acta Crystallogr. Sect. B* **40,** 26 (1984).
6. J. L. Hodeau, Thèse d'Etat, Université Scientifique et Médicale de Grenoble (1984).
7. G. P. Espinosa, *Mater. Res. Bull.* **15,** 791 (1980).
8. M. Marezio, J. P. Remeika, and P. D. Dernier, *Acta Crystallogr. Sect. B* **26,** 2008 (1970).
9. M. Marezio, P. D. Dernier, J. Chenavas, and J. C. Joubert, *J. Solid State Chem.* **6,** 16 (1973).
10. J. Chenavas, J. C. Joubert, M. Marezio, and B. Bochu, *J. Solid State Chem.* **14,** 25 (1975).